Direct imaging of current-driven domain walls in ferromagnetic nanostripes

W. C. Uhlig,[a] M. J. Donahue, D. T. Pierce, and J. Unguris[b]
National Institute of Standards and Technology, Gaithersburg, Maryland 20899-6202, USA

(Received 27 January 2009; accepted 2 April 2009; published online 21 May 2009)

To better understand the response of domain walls to current-induced spin transfer torques, we have directly imaged the internal magnetic structure of domain walls in current-carrying ferromagnetic nanostripes. Domain wall images were acquired both while a constant current was flowing through the wire, and after applying current pulses. Domain walls ranging from vortex walls in wide (1 μm) wires to transverse walls in narrow (100 nm) wires were quantitatively analyzed using scanning electron microscopy with polarization analysis. The domain wall motion is characterized by strong interactions with random pinning sites along the wire. The walls either jump with the electron flow between pinning sites, or the pinned walls are distorted by the current. The domain wall propagation is also associated with transverse motion of the vortex core. [DOI: 10.1063/1.3125526]

I. INTRODUCTION

Current-driven domain wall motion offers the exciting prospect of manipulating magnetization in magnetic nanostructures and devices without applying external magnetic fields.[1–21] The driving force behind current-induced domain wall motion is the quantum mechanical phenomenon of spin transfer torque.[22–26] As spin-polarized electrons pass through a domain wall, a torque is exerted on the electrons tending to align their spin with the magnetization direction. Conservation of angular momentum requires a reaction torque from the electron spin to the magnetization. The ensuing "spin pressure" pushes the wall in the direction of the electron flow, leading to domain wall motion and distortion or transformation of its shape.

Early experiments of Freitas and Berger[2] used the Faraday effect to observe current-induced domain wall displacement in thin $Ni_{80}Fe_{20}$ films. The domain wall motion was in the direction of electron flow in agreement with the theory of Berger.[4] Similar results were found more recently from other experiments on extended films.[5,6] However, the large increased interest in current-induced domain wall motion coincided with moving domains in nanowires because of the prospect of changing the magnetic configuration of nanoelectronic devices. Over the past 5 years, there have been numerous studies of current-induced domain wall motion in ferromagnetic nanowires, typically 5–50 nm thick and 100 nm to several hundreds of nanometers wide, made possible by advances in nanofabricaton techniques. $Ni_{80}Fe_{20}$ is usually chosen because of its very low anisotropy and magnetostriction. In such a nanowire, shape anisotropy dominates magnetocrystalline anisotropy constraining the magnetization to lie along the wire with domains separated by head-to-head or tail-to-tail walls. Various combinations of magnetoresistance, magnetic force microscopy (MFM), and Kerr microscopy measurements have been used to observe current-induced domain wall motion in, for example, ring structures,[7] a spin valve free layer,[8] a wire with nanoconstrictions,[9] and other geometries,[10] including a ferromagnetic semiconductor structure.[11] The results were consistent with the spin transfer torque mechanism.

Yamagouchi *et al.*[12] used MFM to track the distance the domain walls moved in the nanowire during a current pulse and thereby extracted an average velocity and the efficiency for electrons spins to change the magnetic moment of the wire, that is, the number of displaced domain wall spins that are flipped per spin-polarized conduction electron. Similar experiments were carried out by Klaui *et al.*,[15] but in addition, high resolution scanning electron microscopy with polarization analysis (SEMPA) images of the domain walls were acquired before and after the 10 μs pulses. After several pulses the initial vortex wall was transformed to a transverse wall which appeared more strongly pinned. The unexpectedly low domain wall velocity and low spin transfer efficiency of these two experiments is consistent with experiments of Yang and Erskine[19] who measured time resolved domain wall motion for pulses of several μm duration. They found that above a threshold current density, the domain wall motion took place within the first 300 ns (the resolution of their time resolved Kerr microscopy), and therefore was independent of pulse length for pulse duration longer than 300 ns. The importance of domain wall pinning was seen in magnetic transmission x-ray microscopy imaging of domain wall displacement with 1 ns pulses by Meier *et al.*[20] They found that walls moved with high efficiency on some pulses, but with very low efficiency on others, apparently undergoing a stochastic pinning and depinning, which if averaged over a long pulse would lead to a low average velocity. When the pinning potential is nulled by applying an external magnetic field, Beach *et al.*[17] found that the current is far more efficient at translating a wall than pinning-dominated experiments would suggest.

What emerges is a picture of current-driven domain wall displacement in the direction of electron flow that depends on the domain wall configuration and is strongly influenced by the heterogeneous potential landscape due to pinning centers. Velocities and efficiencies measured at the leading edge

[a]Present address: Army Research Laboratory, Aberdeen Proving Ground, Maryland 21005, USA.
[b]Electronic mail: john.unguris@nist.gov.

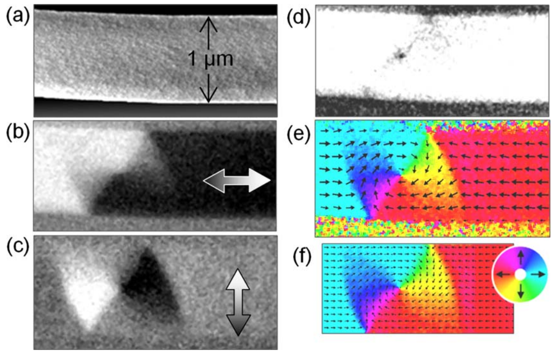

FIG. 1. (Color online) SEMPA measurement of a vortex in a 1 μm wide by 12 nm thick stripe. (a) SEMPA simultaneously images the topography, (b) the in-plane horizontal, and (c) in-plane vertical magnetization components. (d) The in-plane magnetization magnitude and (e) direction are derived from these components, and may be directly compared to the results of (f) a micromagnetics model. The relationship between color and magnetization direction is given by the inset color wheel.

of a current pulse are much higher than the average over a long pulse. The pinning centers give rise to a threshold current required for domain wall displacement and to the nondeterministic nature of the current-induced displacements between pinning centers. Although there is general agreement regarding the physical basis of the spin-transfer-torque-induced domain wall motion and many of the general characteristics, unresolved issues remain, particularly with regard to domain wall pinning. A review of the experimental situation can be found in Ref. 21. Additionally, there are numerous theoretical models that differ in details and ability to quantitatively describe the domain wall behavior.[1–3,27–39] The recent review by Ralph and Stiles[40] gives an update on the current theoretical situation.

In this paper we present images of domain walls in the presence of a current. High spatial resolution (10 nm) images of the magnetic nanostructures were obtained using SEMPA.[41,42] SEMPA images were acquired as a function of applied current for both vortex and transverse walls. The images show motion that is strongly influenced by domain wall pinning. At low currents domain walls are initially distorted, but do not move. At sufficiently large currents, the distortion reaches a break point and the wall is released and propagates along the wire in the direction of the electron flow until it reaches the next pinning site or is swept from the wire. The SEMPA images also reveal structural changes in the domain walls: vortex cores that move transverse to the current, transitions between vortex and transverse walls, and the stabilization of multivortex domain wall states in wider wires.

II. EXPERIMENT

An example of a SEMPA image of a vortex domain wall in a 1 μm wide stripe is shown in Fig. 1. The electron spin polarization analyzers on our SEMPA instrument can simultaneously measure the topography and two components of the magnetization vector, either the two in-plane components or one in-plane and the out-of-plane component. For these measurements, we focus on in-plane magnetization components, as shown in Figs. 1(b) and 1(c). The topography image is shown in Fig. 1(a). These SEMPA images typically take between 5 and 10 min to acquire. From the two magnetization components we can derive the images of the in-plane magnetization magnitude and direction, as shown in Figs. 1(d) and 1(e). The magnitude is uniform except where the magnetization is either out of plane, or where the magnetization is changing direction rapidly relative to the beam size. Both of these effects are responsible for the missing magnetization at the vortex core which produces the small black dot near the center of Fig. 1(d). The in-plane magnetization direction shown in Fig. 1(e) is measured directly and quantitatively. In this paper the magnetization direction in the SEMPA images is represented both by the color map shown in Fig. 1, and by overlaid arrows which are obtained by averaging over several adjacent pixels. Since the magnetization direction is measured directly, the SEMPA images can be unambiguously compared with the results of micromagnetic calculations such as the one shown in Fig. 1(f).

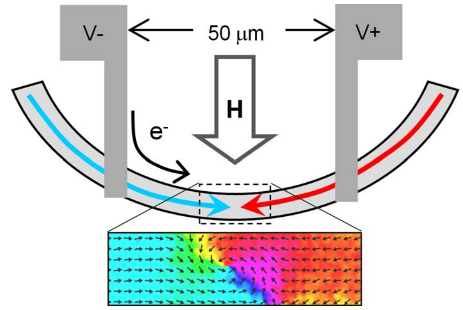

FIG. 2. (Color online) Device schematic showing stripe geometry. Applied currents are defined as positive for electrons flowing from left to right. Domain walls are inserted by momentarily saturating the device with a large field perpendicular to the arc.

The devices in this study consist of wire stripes between 100 nm and 1 μm wide that were patterned using electron beam lithography and lift-off. The wires were made from 12 and 24 nm thick $Ni_{80}Fe_{20}$ films on Si oxide substrates and then capped with a 10 nm Au film to prevent oxidation. After inserting the structures into the SEMPA chamber, the Au layer was removed by ion milling and the samples were coated with a 0.5 nm thick Fe layer to enhance the SEMPA contrast. The wires were patterned as a gradual arc with two aluminum contacts, as shown in Fig. 2. Momentarily applying a magnetic field of 80 kA/m (1000 Oe) perpendicular to the arc nucleates a head-to-head or tail-to-tail domain wall in the middle of the arc. The type of the domain wall nucleated, vortex or transverse, depends on the thickness and width of the stripe.

III. RESULTS: STATIC WALLS

The initial domain wall configurations of our devices agree well with predicted domain wall phase diagrams for magnetic stripes.[43,44] Two basic wall geometries are possible in these stripes: A vortex wall in which the magnetization circulates about a central vortex core that is magnetized perpendicular to the plane. The vortex wall is characterized by the chirality which is the direction, clockwise or counterclockwise, that the magnetization rotates about the core, and the polarity, which is the direction, up or down, that the core

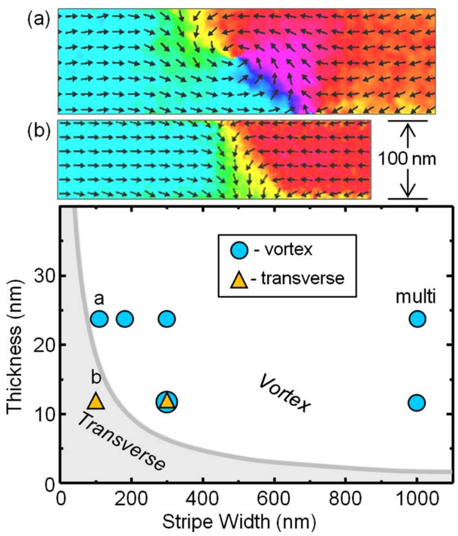

FIG. 3. (Color online) Stripe geometry domain wall phase diagram indicating samples used in this study, and examples of (a) a vortex (135 nm wide by 24 nm thick stripe) and (b) a transverse domain wall (100 nm wide by 12 nm thick stripe).

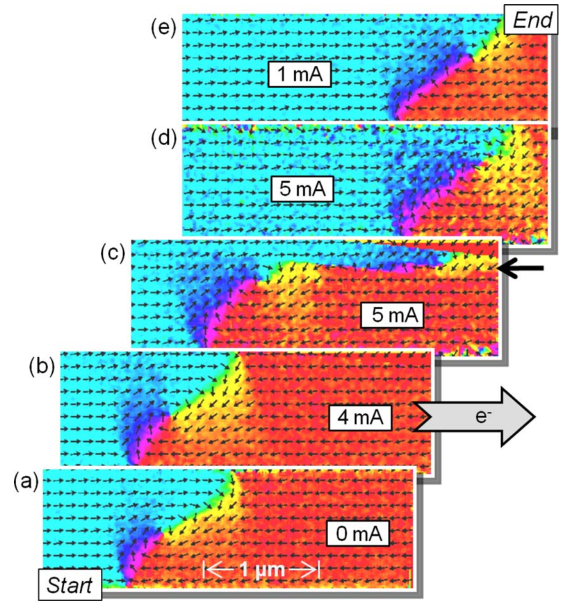

FIG. 4. (Color online) SEMPA images of a vortex wall in a 1 μm wide by 12 nm thick stripe measured while incrementally increasing current. Starting from bottom, the vortex remains pinned as current is increased to 4 mA (3.4×10^{11} A/m^2). After increasing the current to 5 mA (4.2×10^{11} A/m^2), the wall jumps to new pinning site during the image scan (see arrow).

magnetization points relative to the surface. Or a transverse wall which consists of a simple in-plane Neel-like domain wall that is completely described by the chirality of the wall. The region of the stripe phase diagram sampled by our measurements is shown in Fig. 3. Several distinct wall regimes are represented by the data: thin narrow stripes that only contain transverse walls, intermediate width stripes which can support either transverse or vortex walls, or wide stripes which contain only vortex walls. As can be seen from the examples in Fig. 3, the vortex and transverse walls are closely related;[45] cutting the vortex along the stripe length reveals two transverse walls of opposite chirality that are joined at the vortex core.

To analyze the internal domain wall structure while current is flowing through the wire, a series of SEMPA images was acquired while incrementing the current. In general this produced a series of static images of domain walls fixed at pinning sites along the stripe. Topography images were used to properly align the magnetization images. An example of such a series is shown in Fig. 4 for a vortex wall in a 1 μm wide by 12 nm thick stripe. Initially the wall is pinned and there is no obvious movement while increasing the current from 0 to 4 mA. Increasing the current to 5 mA (current density$=4.2\times 10^{11}$ A/m^2) initially moves the wall by 0.7 μm in the direction of electron flow, and then, while scanning the image, the wall jumps another 2.1 μm at the scan line indicated by the arrow. The next scan, repeated with 5 mA still applied, shows the vortex fixed at the new pinning site. Reducing the current to 1 mA shows no obvious further change in position. This same general behavior was observed for most of the stripes: Domain walls remained pinned until reaching fairly high current densities, the walls then jumped from one pinning site to the next. The domain walls moved with the electron flow while the vortex cores moved toward the stripe edge.

To determine if the domain wall structure was being distorted by the electrons flowing through the pinned wall, detailed SEMPA images of the internal domain wall structure at different current densities were compared. The major obstacles to quantitative comparisons are shifts and distortions in the scanned areas between different images. Image distortions are especially significant at the high current densities required to move the walls. High current densities can lead to local heating and small, yet significant, stage drifts during the 5 min required to image a domain wall. To exactly align different magnetization images we used the topographic images that are acquired at the same time as the magnetic images. Gross alignment of images was accomplished by simply shifting different images to align landmarks such as defects. A more accurate correction was obtained by calculating the cross-correlation function between different images to determine shifts and linear scan drifts. An example of this correction is shown in Fig. 5. Initially a reference SEMPA image of the domain wall in this 1 μm$\times$12 nm stripe is acquired with no applied current. The topography image from this reference SEMPA measurement and its self-correlation are shown in Figs. 5(a) and 5(b). The topography images from subsequent SEMPA images at other currents are then cross correlated with the reference image and the two-dimensional shifts and linear distortions are determined. Image shifts move the correlation peak from the correlation image center, while scan distortions stretch the correlation peak. Figure 5(c) shows an image of a vortex wall before compensating for image drift, and Fig. 5(d) shows the resulting, streaked cross-correlation image. Figure 5(e) shows the image after compensating for the image drift, and Fig. 5(f) shows the cross correlation which is almost as sharp as the self-correlation image.

After correcting for image shifts and distortions, we find small but significant wall distortions due to currents flowing

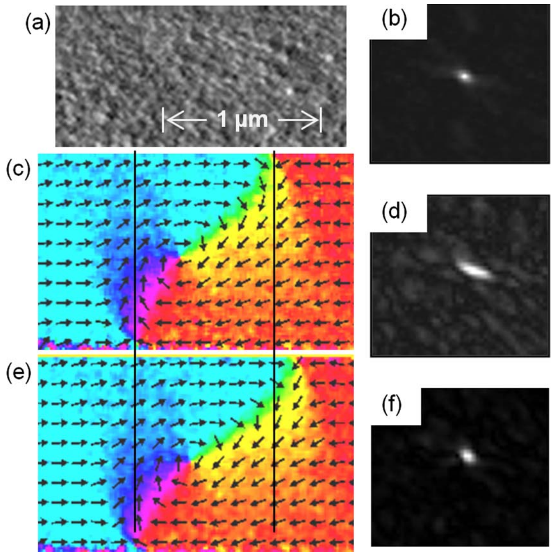

FIG. 5. (Color online) An example of image-drift correction by cross correlation of topography images. (a) Topography images are cross-correlated with reference image and (b) compared to self-correlation. Removing drift from image taken at 3 mA of applied current changes cross correlation from (d) to (f) and magnetization image from (c) to (e).

through the pinned domain walls. These currents are less than the critical currents required to move the domain walls. Examples of these distortions are shown in Fig. 6. The 300 nm wide by 12 nm thick stripe in this case can support either a vortex wall or, after pulsing the current, a transverse wall. Both types of walls are shown with dc flowing in opposite directions to highlight the distortions. Small reversible changes can be observed. For example, in the yellow-colored regions in the vortex and transverse walls the magnetization rotates downward, toward the bottom of the stripe when electrons flow to the left, and in the opposite direction, with

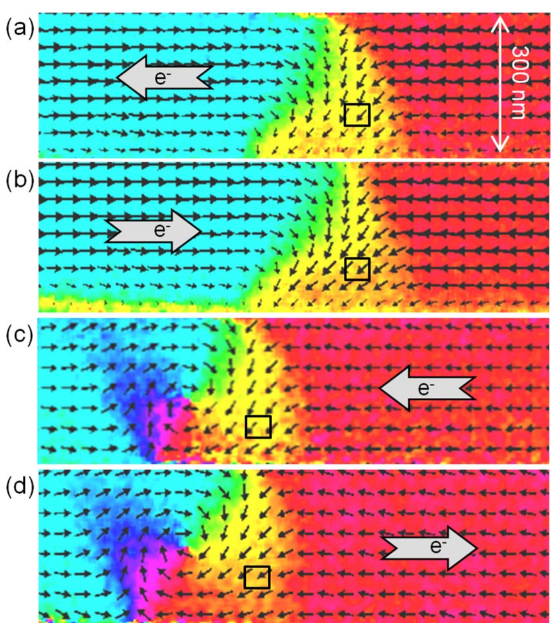

FIG. 6. (Color online) SEMPA images of pinned domain walls in 300 $\times 12$ nm^2 stripes measured from the same areas but with opposite applied currents (transverse: ± 0.5 mA, vortex: ± 1 mA) to highlight distortions of the pinned walls. Boxes indicate sampling regions for Fig. 7.

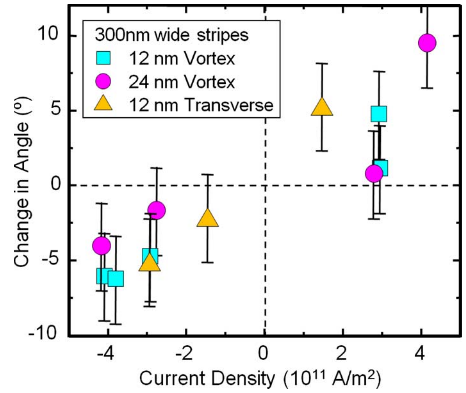

FIG. 7. (Color online) Change in the magnetization direction of a segment of a pinned wall as a function of stripe current. The data are averaged over regions indicated by the boxes in Fig. 6 for the 12 nm thick stripe, and over similar regions for a 24 nm thick sample (not shown). Error bars indicate single standard deviation uncertainties.

electrons flowing to the right. In other words, in this part of the vortex, the magnetization surprisingly tilts away from the electron flow. To get an idea of the magnitude of the effect, the average magnetization direction within the boxed region in the same part of the domain wall is plotted as a function of the current and shown in Fig. 7. The uncertainties in Fig. 7 were determined by how precisely the magnetization direction could be measured in the same size box in a uniformly magnetized part of the stripe far from the domain wall. Although the exact magnitude of the distortion depends on the region of the domain wall that is sampled, all of the pinned domain walls we investigated showed some distortion at currents less than the propagation current. In general, this distortion involved most of the domain wall and was not limited to a specific area. Thus, even though the domain wall may be pinned at a specific point defect, large sections of the domain wall are distorted. The same trends are observed for all the stripes with vortex walls, although a slightly weaker effect is observed in the narrower wires which may be expected due to the greater energy cost associated with deforming the magnetization in a narrower stripe.

The interaction between the magnetization and the magnetic fields generated by the current flowing through the stripes is not the explanation for these distortions. We determined the size of this effect by performing micromagnetic OOMMF (Ref. 46) simulations using applied magnetic fields that were equivalent to the Oersted fields generated by the current. Both pinned walls (pinned by removing cells at the stripe edge near its intersection with the domain wall) and unpinned walls in 12 nm thick by 300 nm wide stripes were simulated using a cell size of $5 \times 5 \times 2$ nm^3. Even with a magnetic field equivalent to an applied current of 2 mA (5.6×10^{11} A/m^2), which was twice as large as the current used in the measurements in Figs. 6(c) and 6(d), the distortions were negligible. The largest change was 0.2° next to the vortex core and less than 0.1° in the outer "wings" of the vortex. The self-generated Oersted fields therefore cannot explain the domain wall distortions.

We have also compared the SEMPA measurements with OOMMF (Ref. 46) simulations which use a modified Landau–Lifschitz–Gilbert equation that contains both adiabatic and

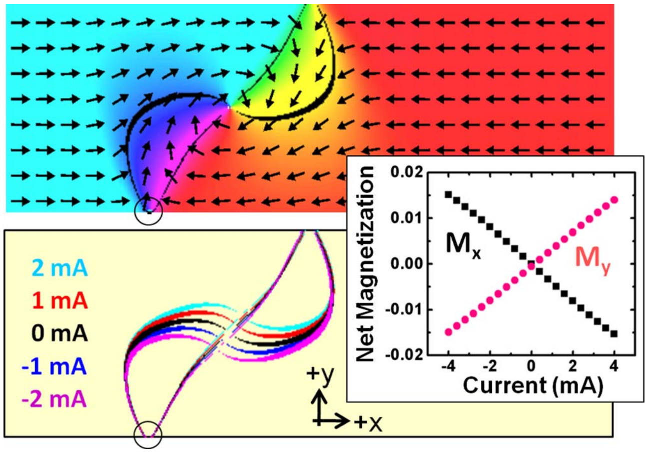

FIG. 8. (Color online) Results from micromagnetics simulations of a 300 $\times 12$ nm^2 stripe pinned by a missing 4 nm wide by 6 nm long notch at the stripe edge (circled). The top panel shows the magnetization at 0 mA. The bottom panel shows contours corresponding to magnetization angles of 45°, 135°, 225°, and 315° as a function of current. The inset shows the net magnetization in the +x and +y directions vs current. The vortex core polarity is out of the page.

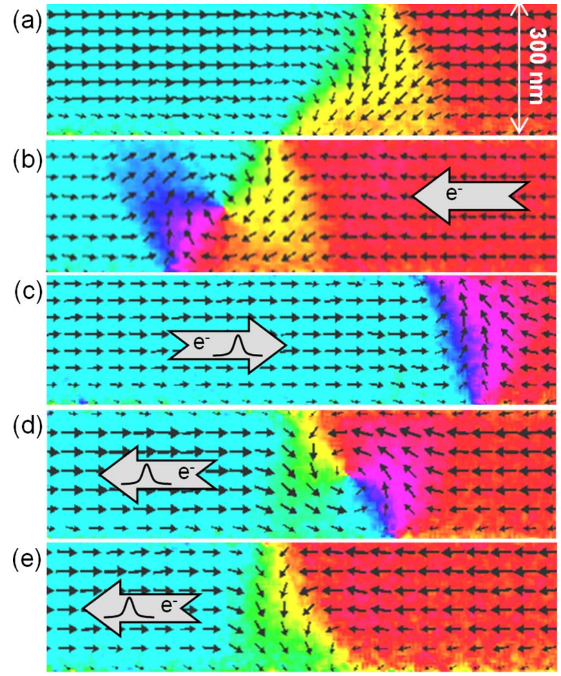

FIG. 9. (Color online) A series of SEMPA images showing distortions and domain wall transitions in a 300×12 nm^2 NiFe wire. (a) The initial transverse wall, which was pinned for applied currents up to -0.5 mA, (b) moves and converts to vortex wall at -1.0 mA. Images (c), (d), and (e) show remanent states after 20 ms current pulses of +1.7, -1.7, and -2.0 mA, respectively. A vortex core is nucleated at the stripe edge in going from (c) to (d) and annihilated at the stripe edge in going from (d) to (e).

nonadiabatic spin-torque terms similar to those in Eq. (3) of Ref. 34. Detailed quantitative comparisons with the experimental results were not possible since we do not know how and where the domain walls are pinned. However, by using some reasonable assumptions, we were able to observe the same current-dependent behavior in some of the models as in the experiments. For example, since defects along the stripe edges may be plausible pinning sites, domain walls were modeled with vortices pinned at a single edge defect. Figure 8 shows the results of such a model calculation for a 300 nm wide by 12 nm thick stripe.[47] The pinning site is a single 6 nm long by 4 nm wide notch at the edge of the stripe. Only the adiabatic spin toque term was included in this calculation, and the polarity of the vortex core is out of the page.

The current-induced distortion of the pinned wall in Fig. 8 agrees qualitatively with the distortions observed in Figs. 6 and 7. We show the current-dependent evolution of the domain wall by plotting the 45°, 135°, 225°, and 315° contours of the pinned wall in Fig. 8. The pinned domain wall remains stationary while the vortex core moves along the wall as the current changes. The direction of the core motion is consistent with an effective force on the core in the $\mathbf{m}_z\times\mathbf{u}_e$ direction, where $\mathbf{m}_z$ is the polarity of the core and $\mathbf{u}_e$ is the direction of electron flow. This type of distortion is consistent with the magnetization tilting away from the electron flow direction as seen in Fig. 7. In fact, it is interesting to note that, for a core with positive polarity, the net magnetization in the +x direction decreases with increasing current, as shown in the inset of Fig. 8. Of course, for a core with negative polarity, the net magnetization in the +x direction would increase.

IV. RESULTS: WALL MOTION

When the applied currents become large enough, the pinned walls break free and move along the stripe to the next pinning site. In the widest and the narrowest stripes this motion does not appear to affect the type of domain wall, but in the intermediate stripes, 300 nm wide by 12 nm thick, the current used to move the wall can also induce transitions from the vortex to the transverse state. This transition has been predicted by micromagnetic simulations,[34,35] and previous measurements have observed transitions induced by current pulses[48] as well as transitions to complex domain states after propagation.[15] The bistable nature of the wall in the 12 nm thick stripe is shown by the series of images in Fig. 9. The initial state in this stripe is the transverse wall shown in Fig. 9(a), which is slightly distorted, but not transformed, by currents of ± 0.5 mA (1.4×10^{11} A/m^2). As the current is increased to -1.0 mA, the wall breaks free of the pinning site, moves in the direction of the electron flow, and stops, ending up as a vortex shown in Fig. 9(b). To further move this domain wall we switch from continuous current to pulsed current to avoid overheating and damaging the wire. Figures 9(c)–9(e) show the remanent states of the domain wall after applying square current pulses of 20 ms duration and of +1.7, -1.7, and -2.0 mA peak amplitudes, respectively.

The SEMPA images of Figs. 9(c)–9(e) give important clues about how the transformation from vortex to transverse state occurs. We find that domain wall motion along the wire stripe is accompanied by motion of the vortex core perpendicular to the stripe edge and the current flow. A vortex wall thus becomes a transverse wall when the current is sufficient to push the vortex core to the stripe edge where it is annihilated, as seen in the transition from Fig. 9(d) and 9(e). Conversely, a vortex may be created by nucleating a vortex core at the intersection of a transverse wall and the stripe edge, such as the transition from Fig. 9(c) and 9(d). We observe that electrons flowing to the left push the domain wall to the left and the vortex core to the bottom of the stripe, while electrons flowing to the right push the wall to the right and the core to the top edge. Thus, the domain wall usually stops as a transverse wall with a chirality that is determined by the direction of electron flow. The same vortex core motion can also be seen in the 1 μm wide stripe shown in Fig. 4, where the core again moves toward the top edge during propagation of the wall to the right.

The direction of this perpendicular vortex core motion in micromagnetic simulations depends on the current direction and the vortex core polarity, i.e., whether the core magnetization is into or out of the film plane.[48,49] The final steady-state (as opposed to intermediate dynamic) position of the vortex core is shifted in the direction of $\mathbf{m}_z \times \mathbf{u}_e$, where $\mathbf{m}_z$ is the orientation of the vortex core, and $\mathbf{u}_e$ is the direction of the electron flow. This part of the motion is determined solely by the adiabatic spin-torque term. The vortex cores of all the initially nucleated vortex walls we imaged in our measurements moved in the same direction relative to the direction of the electron flow. Our experiments do not determine the absolute dependence of the motion on the vortex core polarity since the z-component of the magnetization was not measured. However, if this model of the dynamics is correct, then all of the initially nucleated vortices had the same core polarity with the magnetization pointing out of the plane of the substrate. Such behavior is not surprising given the likely sensitivity of the nucleation to asymmetries in the nucleation procedure, such as the existence of a small out-of-plane field when the domain wall is initially created.

In the smallest structures studied, the 100 nm wide by 12 nm thick stripes, only transverse walls were observed. In fact, the chirality of the transverse wall very rarely changed even with pulsing the current in different directions and after multiple propagation events. The chirality of the transverse wall only reversed twice in 15 events, in stark contrast to the consistent reversals observed in the 300 nm wide devices. This may indicate that in the narrower 100 nm wide walls the probability of injecting a vortex core from the edge during motion is less likely and the wall motion is simpler, without transitions between vortex and transverse walls. This observed switching behavior may also be related to recent measurements by Vanhaverbeke *et al.*[50] of domain wall propagation in $Ni_{70}Fe_{30}/Fe$ bilayers which indicate that an additional 2 nm thick Fe film eliminates the randomness of the final state after pulsing the current.

Finally, in the largest structures studied, the 1 μm wide by 24 nm thick stripes, moving the initial lone vortex wall can lead to the generation of complex multiple vortex walls. An example of this transition is shown in Fig. 10 where the initial single vortex state is transformed into a wall with three vortices after using a relatively low current density of 2×10^{11} A/m^2 to push the wall to the electrical contact and back. The resulting domain wall structure is a cross-tie wall consisting of alternating vortices and antivortices. Cross-tie domain walls are the minimum energy domain wall for NiFe films of this thickness.[51] The multivortex domain wall in Fig. 10 is strongly pinned by a major defect that is clearly visible in the topography image. By comparing the SEMPA images taken during opposite electron flows, Figs. 10(b) and 10(c), and using the vertical reference lines to locate the vortices (lines 2–4) and end points (lines 1 and 5) of the domain wall, one can see that the multivortex wall is distorted in much the same way as a single vortex. The overall size of the domain wall does not change, and the vortex and antivortex pinned by the large defect (near line 4) do not move; however, the unpinned vortex cores (lines 2 and 3) move along the domain wall toward the stripe edge. Furthermore, comparison of similar areas such as the ones in the boxes in Figs. 10(b) and 10(c) reveals that the magnetization away from the vortex cores rotates in the same direction relative to the electron flow as in the single vortex nanostripes shown in Fig. 6.

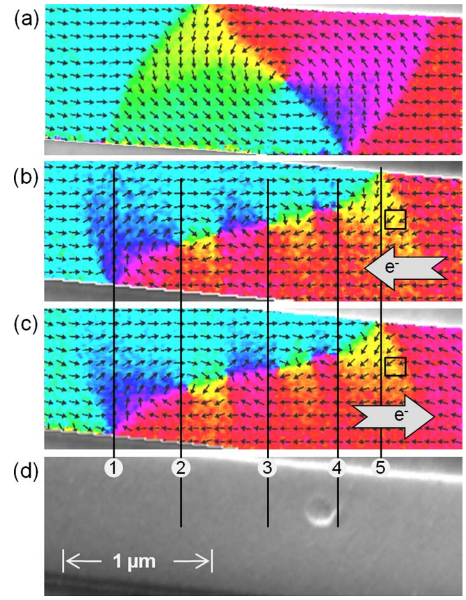

FIG. 10. (Color online) SEMPA images of domain wall transitions in a 1 μm $\times$ 24 nm stripe. After moving a large distance, (a) the initial vortex is transformed to a multivortex domain wall pinned at the large defect visible in (d). Magnetization images (b) and (c) from the same areas but with opposite currents ($\pm$5 mA) show the vortex cores moving along the pinned domain wall. The vertical reference lines help locate the vortices and the wall end points.

V. CONCLUSION

In this work we have imaged spin-induced domain wall distortions and motion in ferromagnetic stripes whose sizes span three distinct domain wall regimes: vortex walls in 1 μm wide wires, bistable vortex or transverse walls in 300 nm wide wires, and transverse walls in 100 nm wide wires. At current densities lower than current densities required for domain wall propagation, the pinned walls show elastic distortions of both vortex and transverse walls due to current flowing through the stripes. The observed distortions appear to be an intrinsic effect with a distinctive tilting of the wall magnetization which is independent of the pinning site. We have been able to qualitatively reproduce some of these distortions using micromagnetic simulations which include presently accepted models of spin transfer torques. A quantitative comparison was not possible because we do not know the location and strength of pinning sites in these stripes. This work underscores the significance of pinning sites in current-induced, spin-torque driven domain wall motion. Identifying and controlling these sites may provide a path toward domain wall manipulation using lower current densities.

ACKNOWLEDGMENTS

The authors thank Mark Stiles, Hongki Min, and Robert McMichael for many helpful discussions. This work was supported in part by the Office of Naval Research. Research performed at the NIST Center for Nanoscale Science and Technology.

[1] L. Berger, J. Appl. Phys. **49**, 2156 (1978).
[2] P. P. Freitas and L. Berger, J. Appl. Phys. **57**, 1266 (1985).
[3] S. S. P. Parkin, M. Hayashi, and L. Thomas, Science **320**, 190 (2008).
[4] L. Berger, J. Appl. Phys. **55**, 1954 (1984).
[5] L. Gan, S. H. Chung, K. H. Aschenbach, M. Dreyer, and R. D. Gomez, IEEE Trans. Magn. **36**, 3047 (2000).
[6] H. Koo, C. Krafft, and R. D. Gomez, Appl. Phys. Lett. **81**, 862 (2002).
[7] M. Klaui, C. A. F. Vaz, J. A. C. Bland, W. Wernsdorfer, G. Faini, E. Cambril, and L. J. Heyderman, Appl. Phys. Lett. **83**, 105 (2003).
[8] J. Grollier, P. Boulenc, V. Cros, A. Hamzic, A. Vaures, A. Fert, and G. Faini, Appl. Phys. Lett. **83**, 509 (2003).
[9] M. Tsoi, R. E. Fontana, and S. S. P. Parkin, Appl. Phys. Lett. **83**, 2617 (2003).
[10] N. Vernier, D. A. Allwood, D. Atkinson, M. D. Cooke, and R. P. Cowburn, Europhys. Lett. **65**, 526 (2004).
[11] M. Yamanouchi, D. Chiba, F. Matsukura, and H. Ohno, Nature (London) **428**, 539 (2004).
[12] A. Yamaguchi, T. Ono, S. Nasu, K. Miyake, K. Mibu, and T. Shinjo, Phys. Rev. Lett. **92**, 077205 (2004).
[13] C. K. Lim, T. Devolder, C. Chappert, J. Grollier, V. Cros, A. Vaurès, A. Fert, and G. Faini, Appl. Phys. Lett. **84**, 2820 (2004).
[14] S. H. Florez, C. Krafft, and R. D. Gomez, J. Appl. Phys. **97**, 10C705 (2005).
[15] M. Kläui, P.-O. Jubert, R. Allenspach, A. Bischof, J. A. C. Bland, G. Faini, U. Rüdiger, C. A. F. Vaz, L. Vila, and C. Vouille, Phys. Rev. Lett. **95**, 026601 (2005).
[16] M. Kläui, M. Laufenberg, L. Heyne, D. Backes, U. Rüdiger, C. A. F. Vaz, J. A. C. Bland, L. J. Heyderman, S. Cherifi, A. Locatelli, T. O. Mentes, and L. Aballe, Appl. Phys. Lett. **88**, 232507 (2006).
[17] G. S. D. Beach, C. Knutson, C. Nistor, M. Tsoi, and J. L. Erskine, Phys. Rev. Lett. **97**, 057203 (2006).
[18] M. Hayashi, L. Thomas, C. Rettner, R. Moriya, X. Jiang, and S. S. P. Parkin, Phys. Rev. Lett. **97**, 207205 (2006).
[19] S. Q. Yang and J. L. Erskine, Phys. Rev. B **75**, 220403 (2007).
[20] G. Meier, M. Bolte, R. Eiselt, B. Krüger, D. H. Kim, and P. Fischer, Phys. Rev. Lett. **98**, 187202 (2007).
[21] G. S. D. Beach, M. Tsoi, and J. L. Erskine, J. Magn. Magn. Mater. **320**, 1272 (2008).
[22] L. Berger, Phys. Rev. B **54**, 9353 (1996).
[23] L. Berger, J. Appl. Phys. **81**, 4880 (1997).
[24] J. C. Slonczewski, J. Magn. Magn. Mater. **159**, L1 (1996).
[25] J. C. Slonczewski, J. Magn. Magn. Mater. **195**(2), 261 (1999).
[26] M. D. Stiles and A. Zangwill, Phys. Rev. B **66**, 014407 (2002).
[27] G. Tatara and H. Kohno, Phys. Rev. Lett. **92**, 086601 (2004).
[28] X. Waintal and M. Viret, Europhys. Lett. **65**, 427 (2004).
[29] Z. Li and S. Zhang, Phys. Rev. Lett. **92**, 207203 (2004).
[30] S. Zhang, P. M. Levy, and A. Fert, Phys. Rev. Lett. **88**, 236601 (2002).
[31] S. Zhang and Z. Li, Phys. Rev. Lett. **93**, 127204 (2004).
[32] Z. Li and S. Zhang, Phys. Rev. B **70**, 024417 (2004).
[33] A. Thiaville, Y. Nakatani, J. Miltat, and N. Vernier, J. Appl. Phys. **95**, 7049 (2004).
[34] A. Thiaville, Y. Nakatani, J. Miltat, and Y. Suzuki, Europhys. Lett. **69**, 990 (2005).
[35] S. E. Barnes and S. Maekawa, Phys. Rev. Lett. **95**, 107204 (2005).
[36] J. He, Z. Li, and S. Zhang, Phys. Rev. B **73**, 184408 (2006).
[37] J. Shibata, Y. Nakatani, G. Tatara, H. Kohno, and Y. Otani, Phys. Rev. B **73**, 020403(R) (2006).
[38] J. A. Xiao, A. Zangwill, and M. D. Stiles, Phys. Rev. B **73**, 054428 (2006).
[39] M. D. Stiles, W. M. Saslow, M. J. Donahue, and A. Zangwill, Phys. Rev. B **75**, 214423 (2007).
[40] D. C. Ralph and M. D. Stiles, J. Magn. Magn. Mater. **320**, 1190 (2008).
[41] M. R. Scheinfein, J. Unguris, M. H. Kelley, D. T. Pierce, and R. J. Celotta, Rev. Sci. Instrum. **61**, 2501 (1990).
[42] J. Unguris, in *Magnetic Imaging and Its Applications to Materials*, edited by M. De Graef and Y. Zhu (Academic, Burlington, MA, 2000), Vol. 36.
[43] R. D. McMichael and M. J. Donahue, IEEE Trans. Magn. **33**, 4167 (1997).
[44] Y. Nakatani, A. Thiaville, and J. Miltat, J. Magn. Magn. Mater. **290-291**, 750 (2005).
[45] O. Tchernyshyov and G. W. Chern, Phys. Rev. Lett. **95**, 197204 (2005).
[46] M. J. Donahue and D. J. Porter, *OOMMF's User Guide, Version 1.0, NISTIR 6376* (National Institute of Standards and Technology, Gaithersburg, MD, 1999).
[47] In the simulations: cell size $=2\times2\times12$ nm^3, $M_s=8\times10^5$ A/m, $A=10\times10^{-12}$ J/m, and an easy axis anisotropy of 50 mT are included to match the experimental wall width.
[48] L. Heyne, M. Klaui, D. Backes, T. A. Moore, S. Krzyk, U. Rudiger, L. J. Heyderman, A. F. Roriguez, F. Nolting, T. O. Mentes, M. A. Nino, A. Locatelli, K. Kirsch, and R. Mattheis, Phys. Rev. Lett. **100**, 066603 (2008).
[49] S.-M. Seo, K.-J. Lee, W.-K. Kim, and T.-D. Lee, Appl. Phys. Lett. **90**, 252508 (2007).
[50] A. Vanhaverbeke, A. Bischof, and R. Allenspach, Phys. Rev. Lett. **101**, 107202 (2008).
[51] A. Hubert and R. Schäfer, *Magnetic Domains: The Analysis of Magnetic Microstructures* (Springer-Verlag, Berlin, 1998).